Optical magnetic field mapping using a subwavelength aperture

Hyun Woo Kihm,[1,6,*] Jineun Kim,[2,6] Sukmo Koo, [3] Jaesung Ahn, [1] Kwangjun Ahn,[4] Kwanggeol Lee,[5] Namkyoo Park,[3] and Dai-Sik Kim[1]

[1]*Center for Subwavelength Optics and Department of Physics and Astronomy, Seoul National University, Seoul, 151-747, Korea*
[2]*Samsung Advanced Institute of Technology, Yongin, 446-712, Korea*
[3]*Photonic Systems Laboratory, School of EECS, Seoul National University, Seoul, 151-747, Korea*
[4]*Global Frontier Center for Multiscale Energy Systems, Seoul National University, Seoul, 151-747, Korea*
[5]*Department of Physics, Hanyang University, Seoul, 133-791, Korea*
[6]*These authors contributed equally.*
**hw.kihm@gmail.com*

Abstract: Local distribution of the optical magnetic field is a critical parameter in developing materials with artificially engineered optical properties. Optical magnetic field characterization in nano-scale remains a challenge, because of the weak matter-optical magnetic field interactions. Here, we demonstrate an experimental visualization of the optical magnetic field profiles by raster scanning circular apertures in metal film or in a conical probe. Optical magnetic fields of surface plasmon polaritons and radially polarized beam are visualized by measuring the transmission through metallic apertures, in excellent agreements with theoretical predictions. Our results show that Bethe-Bouwkamp aperture can be used in visualizing optical magnetic field profiles.

OCIS codes: (260.2110) Electromagnetic Optics; (310.6628) Subwavelength structures, nanostructures.

References and links

1. J. D. Jackson, *Classical Electrodynamics, 3rd edition ed.* (John Wiley & Sons, Inc, New York, 1999).
2. R. A. Shelby, D. R. Smith, and S. Schultz, "Experimental verification of a negative index of refraction," Science **292**(5514), 77–79 (2001).
3. J. Valentine, S. Zhang, T. Zentgraf, E. Ulin-Avila, D. A. Genov, G. Bartal, and X. Zhang, "Three-dimensional optical metamaterial with a negative refractive index," Nature **455**(7211), 376–379 (2008).
4. N. Engheta, "Circuits with light at nanoscales: optical nanocircuits inspired by metamaterials," Science **317**(5845), 1698–1702 (2007).
5. J. B. Pendry, A. J. Holden, D. J. Robbins, and W. J. Stewart, ""Magnetism from conductors and enhanced nonlinear phenomena," IEEE," T. Microw. Theory **47**(11), 2075–2084 (1999).
6. N. Liu, H. Guo, L. Fu, S. Kaiser, H. Schweizer, and H. Giessen, "Three-dimensional photonic metamaterials at optical frequencies," Nat. Mater. **7**(1), 31–37 (2008).
7. J. B. Pendry, "Negative refraction makes a perfect lens," Phys. Rev. Lett. **85**(18), 3966–3969 (2000).
8. S. Koo, M. S. Kumar, J. Shin, D. Kim, and N. Park, "Extraordinary magnetic field enhancement with metallic nanowire: role of surface impedance in Babinet's principle for sub-skin-depth regime," Phys. Rev. Lett. **103**(26), 263901 (2009).
9. S.-Y. Lee, I.-M. Lee, J. Park, S. Oh, W. Lee, K.-Y. Kim, and B. Lee, "Role of magnetic induction currents in nanoslit excitation of surface plasmon polaritons," Phys. Rev. Lett. **108**(21), 213907 (2012).
10. K. Lee, M. Yi, S. E. Park, and J. Ahn, "Phase-shift anomaly caused by subwavelength-scale metal slit or aperture diffraction," Opt. Lett. **38**(2), 166–168 (2013).
11. A. Asenjo-Garcia, A. Manjavacas, V. Myroshnychenko, and F. J. García de Abajo, "Magnetic polarization in the optical absorption of metallic nanoparticles," Opt. Express **20**(27), 28142–28152 (2012).
12. J. H. Kang, D. S. Kim, and Q. H. Park, "Local capacitor model for plasmonic electric field enhancement," Phys. Rev. Lett. **102**(9), 093906 (2009).
13. K. G. Lee, H. W. Kihm, J. E. Kihm, W. J. Choi, H. Kim, C. Ropers, D. J. Park, Y. C. Yoon, S. B. Choi, D. H. Woo, J. Kim, B. Lee, Q. H. Park, C. Lienau, and D. S. Kim, "Vector field microscopic imaging of light," Nat. Photonics **1**(1), 53–56 (2007).

#181418 - $15.00 USD Received 10 Dec 2012; revised 16 Jan 2013; accepted 23 Jan 2013; published 28 Feb 2013

14. D.-S. Kim, J. Heo, S.-H. Ahn, S. W. Han, W. S. Yun, and Z. H. Kim, "Real-space mapping of the strongly coupled plasmons of nanoparticle dimers," Nano Lett. **9**(10), 3619–3625 (2009).
15. L. Novotny, M. R. Beversluis, K. S. Youngworth, and T. G. Brown, "Longitudinal field modes probed by single molecules," Phys. Rev. Lett. **86**(23), 5251–5254 (2001).
16. M. Burresi, D. van Oosten, T. Kampfrath, H. Schoenmaker, R. Heideman, A. Leinse, and L. Kuipers, "Probing the magnetic field of light at optical frequencies," Science **326**(5952), 550–553 (2009).
17. N. Kumar, A. C. Strikwerda, K. Fan, X. Zhang, R. D. Averitt, P. C. M. Planken, and A. J. L. Adam, "THz near-field Faraday imaging in hybrid metamaterials," Opt. Express **20**(10), 11277–11287 (2012).
18. T. H. Taminiau, S. Karaveli, N. F. van Hulst, and R. Zia, "Quantifying the magnetic nature of light emission," Nat Commun **3**, 979 (2012).
19. S. Karaveli and R. Zia, "Spectral tuning by selective enhancement of electric and magnetic dipole emission," Phys. Rev. Lett. **106**(19), 193004 (2011).
20. M. A. Seo, A. J. L. Adam, J. H. Kang, J. W. Lee, S. C. Jeoung, Q. H. Park, P. C. M. Planken, and D. S. Kim, "Fourier-transform terahertz near-field imaging of one-dimensional slit arrays: mapping of electric-field-, magnetic-field-, and Poynting vectors," Opt. Express **15**(19), 11781–11789 (2007).
21. A. Bitzer, H. Merbold, A. Thoman, T. Feurer, H. Helm, and M. Walther, "Terahertz near-field imaging of electric and magnetic resonances of a planar metamaterial," Opt. Express **17**(5), 3826–3834 (2009).
22. E. Devaux, A. Dereux, E. Bourillot, J.-C. Weeber, Y. Lacroute, J.-P. Goudonnet, and C. Girard, "Local detection of the optical magnetic field in the near zone of dielectric samples," Phys. Rev. B **62**(15), 10504–10514 (2000).
23. H. W. Kihm, S. M. Koo, Q. H. Kim, K. Bao, J. E. Kihm, W. S. Bak, S. H. Eah, C. Lienau, H. Kim, P. Nordlander, N. J. Halas, N. K. Park, and D. S. Kim, "Bethe-hole polarization analyser for the magnetic vector of light," Nat Commun **2**, 451 (2011).
24. H. A. Bethe, "Theory of diffraction by small holes," Phys. Rev. **66**(7-8), 163–182 (1944).
25. C. J. Bouwkamp, "Diffraction theory," Rep. Prog. Phys. **17**(1), 35–100 (1954).
26. A. Y. Nikitin, F. J. García-Vidal, and L. Martín-Moreno, "Surface electromagnetic field radiated by a subwavelength hole in a metal film," Phys. Rev. Lett. **105**(7), 073902 (2010).
27. J. M. Yi, A. Cuche, F. de León-Pérez, A. Degiron, E. Laux, E. Devaux, C. Genet, J. Alegret, L. Martín-Moreno, and T. W. Ebbesen, "Diffraction regimes of single holes," Phys. Rev. Lett. **109**(2), 023901 (2012).
28. M. Stalder and M. Schadt, "Linearly polarized light with axial symmetry generated by liquid-crystal polarization converters," Opt. Lett. **21**(23), 1948–1950 (1996).
29. L. Novotny and B. Hecht, *Principles of Nano-Optics* (Cambridge University press, 2006).
30. M. Liu, T.-W. Lee, S. K. Gray, P. Guyot-Sionnest, and M. Pelton, "Excitation of dark plasmons in metal nanoparticles by a localized emitter," Phys. Rev. Lett. **102**(10), 107401 (2009).
31. F. Hao, Y. Sonnefraud, P. V. Dorpe, S. A. Maier, N. J. Halas, and P. Nordlander, "Symmetry breaking in plasmonic nanocavities: subradiant LSPR sensing and a tunable Fano resonance," Nano Lett. **8**(11), 3983–3988 (2008).
32. D. J. Park, K. G. Lee, H. W. Kihm, Y. M. Byun, D. S. Kim, C. Ropers, C. Lienau, J. H. Kang, and Q. H. Park, "Near-to-far-field spectral evolution in a plasmonic crystal: Experimental verification of the equipartition of diffraction orders," Appl. Phys. Lett. **93**(7), 073109–073103 (2008).
33. D. J. Park, S. B. Choi, K. J. Ahn, D. S. Kim, J. H. Kang, Q. H. Park, M. S. Jeong, and D. K. Ko, "Experimental verification of surface plasmon amplification on a metallic transmission grating," Phys. Rev. B **77**(11), 115451 (2008).
34. D. C. Kohlgraf-Owens, S. Sukhov, and A. Dogariu, "Discrimination of field components in optical probe microscopy," Opt. Lett. **37**(17), 3606–3608 (2012).
35. H. W. Kihm, K. G. Lee, D. S. Kim, and K. J. Ahn, "Dual mode near-field scanning optical microscopy for near-field imaging of surface plasmon polariton," Opt. Commun. **282**(12), 2442–2445 (2009).
36. H. Raether, *Surface Plasmons on Smooth and Rough Surfaces and on Gratings* (Springer-Verlag Berlin HeidelBerg, Berlin, 1988).

1. Introduction

Electric and magnetic fields are two main vectors which describe the optical phenomena on the basis of Maxwell's equations. In the theoretical point of view, both electric and magnetic field vectors are equally important as they are closely related to each other through space-time dependent differential equations. In the experimental point of view, magnetic field is often neglected compared to the electric field when describing optical phenomena. This is mainly because the detection of optical magnetic field has been elusive, because it interacts with matter weakly owing to the relative magnetic permeability of $\mu = 1$ at optical frequencies [1]. As a consequence, detectors made of materials in nature barely see the optical magnetic field.

Recently, with the possibility of engineering the optical properties of materials, the knowledge on optical magnetic field becomes important because the refractive index of the material is determined by both electric permittivity and magnetic permeability. Designing

#181418 - $15.00 USD Received 10 Dec 2012; revised 16 Jan 2013; accepted 23 Jan 2013; published 28 Feb 2013

artificial material -so called metamaterial- has attracted surge of interest in optical society because it can achieve extraordinary optical properties, such as negative refractive index [2–6]. In practical point of view, it holds promise in realizing groundbreaking devices such as flat-perfect lens, which may overcome diffraction limit of optics [7]. On the other hands, it is also demonstrated that the role of magnetic field induction in metallic nanostructure plays a crucial role in basic optical phenomena such as transmission and absorption [8–12]. Despite the importance of the information on the local distribution of electric and magnetic fields in nano-scale, it has been challenging to measure the optical magnetic field, unlike the optical electric fields which has been readily measurable with materials with dielectric permittivity $|\varepsilon|$ larger than one [13–15]. The advances in nano-optics and nano-technologies made it feasible to detect optical magnetic field using various schemes: a split-ring resonator structure indented probe [16,17], magnetic dipole transition allowed emitters [18,19], Fourier transform of time-domain measurement of electric field [20,21] and a nanoprobe with the aperture at the metal coated flat bottom [22,23]. Especially, nanostructures, such as a split ring resonator [16] or a circular hole [23], are indented at the apex of the metal coated probes to demonstrate the direct measurements of the optical magnetic field. With the possibility of optical magnetic field 'sensing' with nano-structures, we pursue the next logical step: 'mapping' of optical magnetic field.

In this paper, we demonstrate that the subwavelength aperture punctured in a metal surface can be used for optical magnetic field mapping. In the far-field regime, radial/azimuthal polarized beam [15] with non-trivial local distribution of electric and magnetic field is measured by raster scanning the beam cross section with the apertures punctured in a flat metal film and in a conical probe with flat-bottom apex. Both types of apertures show the predominant coupling of optical magnetic field into the aperture. Also, standing wave pattern of surface confined modes of electric and magnetic fields, so called surface plasmon polariton (SPP), is measured in the near-field regime by using the aperture in the conical probe with flat-bottom apex which was able to approach on the film surface.

2. Experiment and Discussion

To understand the underlying physics in the detection of the optical magnetic field through a subwalvength hole on a metal film, we first give our attention to the boundary condition of electromagnetic field on a good conducting metal. Surface boundary approximation dictates that the interference between the incident and the reflected electromagnetic field makes the tangential component of the electric field on a metal surface to be suppressed by $\sqrt{1/\varepsilon}$ times to the tangential magnetic field strength. On the other hands, the normal component of the electric field is enhanced as surface charge is accumulated on the dielectric-conductor boundary. In turn, the effective magnetic dipole m_{eff} in tangential direction (Fig. 1(a)) and the electric dipole p_{eff} in normal direction (Fig. 1(b)) play dominant roles in transmission of the fields through a subwavelength aperture on a good conducting metal film. The Bethe-Bouwkamp theory accounts for the transmission through small holes for the ideal case where the aperture exists on a perfectly conducting, infinitesimally thin flat metal film [1,24,25]. In quasi-static regime, where the aperture size is very small compared to the wavelength, the model indicates that the transmission can be approximated by the radiation from the effective dipoles m_{eff} and p_{eff} in the aperture. When the transmission is measured by a detector located in the axis normal to the surface, only the radiation from the tangential magnetic dipole can reach the detector in far-field as shown in Fig. 1(c), whereas the normal electric dipole does not radiate towards the detector (Fig. 1(d)). With more realistic conditions, non-PEC metal plane with a finite thickness, Bethe-Bouwkamp approximation with effective dipoles m_{eff} and p_{eff} is no more valid as the other factors begins to play role in the transmission, such as surface plasmon and waveguiding mode [26,27]. In this paper, we will demonstrate the experimental optical magnetic field mapping using a small aperture in metal plane and near-field optical

#181418 - $15.00 USD Received 10 Dec 2012; revised 16 Jan 2013; accepted 23 Jan 2013; published 28 Feb 2013

probe, which supports that the transmission through the aperture is still sensitive to the optical magnetic polarization [23] despite non-ideal conditions.

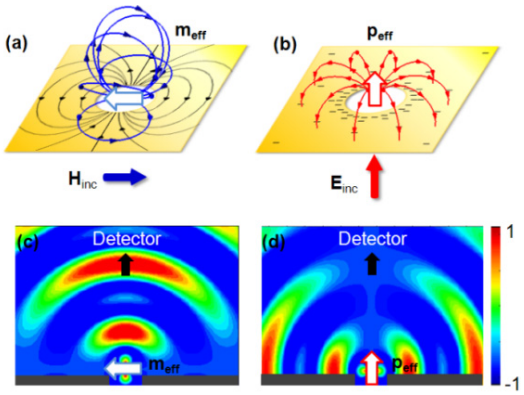

Fig. 1. Bethe's subwavelength aperture on metal surface, creating (a) eddy-current induced effective magnetic dipole (m_{eff}) fields (blue lines) or (b) charge-driven electric dipole (p_{eff}) fields (red lines). Black lines in (a) indicate eddy current distribution. Two dimensional radiation patterns of (c) the effective tangential magnetic dipole and (d) the effective normal electric dipole.

Optical magnetic field detection through a Bethe-Bouwkamp's hole is demonstrated by raster scanning the radial and azimuthal polarized beam with an 80 nm diameter hole punctured in an 80 nm thick gold film deposited on a sapphire substrate (Fig. 2(a)). A theta-cell (Radial Polarization Converter, ARCoptix) generates an incident radially or azimuthally polarized beam at 780 nm wavelength which is focused into an area of 7 μm^2 by an objective lens. Electric and magnetic field components of these loosely focused cylindrically polarized beams have distinguishable spatial distribution from each other [28]. Incident beam is highly tilted by $\theta_{inc} = 82^\circ$ from the axis normal to the metal surface as shown in Fig. 2(a). The transmitted signal is collected by a long working distance objective lens (Mitutuyo x20, NA 0.42), and the intensity is recorded by an avalanche photodiode (Hamamatsu C4777-01) positioned along the axis normal to the metal surface. The cross section of the incident beam profile is raster scanned by moving the aperture in the y-z plane. The y-z plane is tilted by 8° from the aperture metal plane making it normal to the incident beam axis. Electric/magnetic field distributions of radial/azimuthal polarized beam profiles are electrically switchable by using a theta-cell without changing the beam alignment. Tangential magnetic field (H_y) intensity profiles of the radially/azimuthally polarized beam cross sections are plotted following the analytical beam equations (Figs. 2(b), 2(e)) [15,29]. Finite difference time domain (FDTD) calculation of the transmission through the raster scanning aperture (Figs. 2(c), 2(f)) is showing good agreements with experimental results (Figs. 2(d), 2(g)). They clearly demonstrate that the tangential magnetic field is predominantly detected through a small hole.

#181418 - $15.00 USD Received 10 Dec 2012; revised 16 Jan 2013; accepted 23 Jan 2013; published 28 Feb 2013

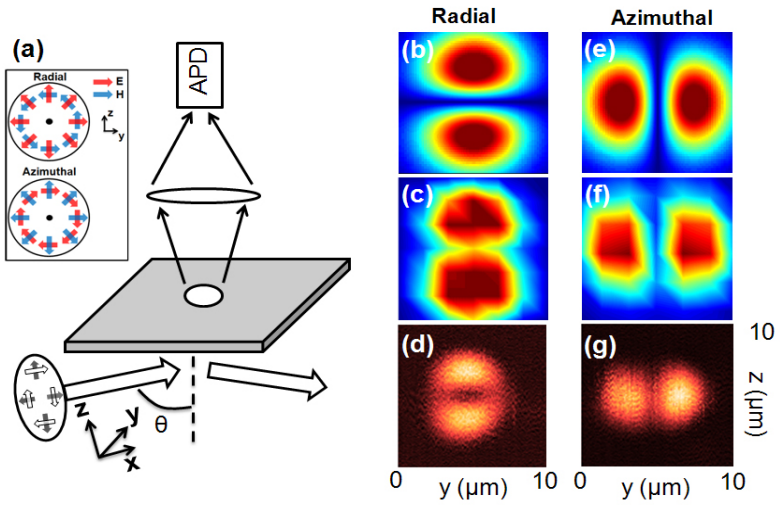

Fig. 2. (a) Transmitted field intensity through the aperture is measured in far-field region while raster scanning the aperture over the beam cross section in y-z plane. (inset) The local distribution of electric and magnetic field for radially/azimuthally polarized beam are depicted in the beam profile cross section. (b, e) Horizontal magnetic field intensity of the radially/azimuthally polarized beams. (c, f) Horizontal magnetic field intensity profile calculated from FDTD simulation of transmission through the aperture which is raster scanning the beam cross section, and (d, g) its experimentally measurement.

As the next step, a subwavelength hole is fabricated at the apex of metal coated conical fiber for magnetic field mapping. The polarization of the transmitted light through the probe is characterized to determine whether the probe is optical magnetic or electric field sensitive [23]. We cut the end edge of the commercial aluminum coated NSOM probe (Nanonics) from the side by using focused ion beam milling, resulting in a flat-bottom facet. The size of the aperture is controlled by the milling position of the probe, which gives smaller aperture size with a closer milling position to the apex. The probes are fabricated to have the nominal ratio of metal thickness to aperture size of about three which is shown to be optical magnetic polarization sensitive as characterized below. It should be noted that the metal thickness around the aperture and the flat-bottom apex are crucial to make the probe sensitive to the optical magnetic field polarization. To characterize the probe, the transmitted polarization is measured while rotating the incident polarization impinging with large oblique incidence angle (Fig. 3(a)). Due to the oblique incidence angle, the polarization of electric and magnetic fields projected on the aperture plane becomes non-orthogonal to each other making it possible to separate the effect of electric and magnetic fields on the transmission through the aperture [23]. The incident polarization is set as TM ($\theta = 45^\circ$ in Fig. 3(b)) and TE ($\theta = 90^\circ$) by rotating the half-wave plate, where the incident magnetic or electric field is parallel to the flat-bottom plane of the probe, respectively. The transmission polarization is fitted with the incident polarizations projected onto the flat-bottom plane of the probe to determine the field component that contributes predominantly in the transmission. With the fitting parameter of incident angle $\theta_{inc} = 84^\circ$, a good agreement is shown between the measured transmission polarization and the magnetic field polarization projected on the probe apex plane (Fig. 3(b)). This observation indicates that the aperture on the apex of the conical probe with flat-bottom still works as an optical magnetic polarizer which favors the coupling with the optical magnetic field. This trait makes this probe well-suited to visualize local distribution of optical magnetic fields.

#181418 - $15.00 USD Received 10 Dec 2012; revised 16 Jan 2013; accepted 23 Jan 2013; published 28 Feb 2013

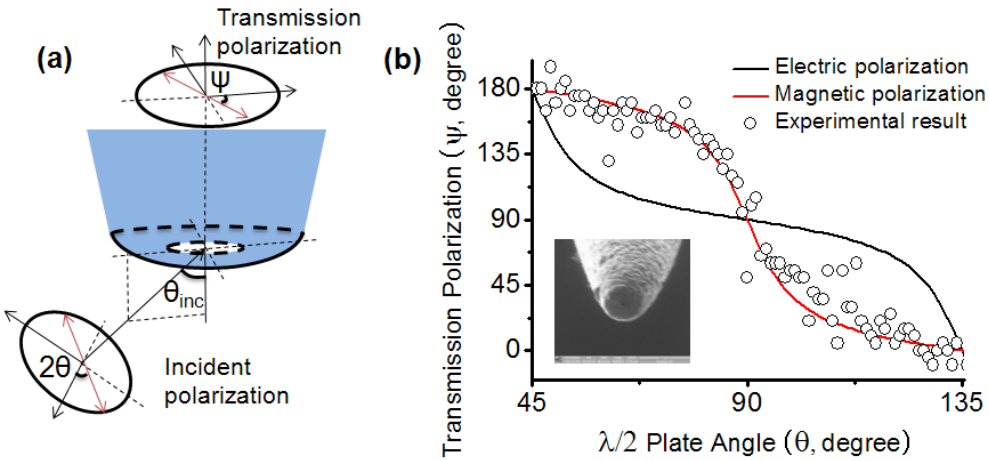

Fig. 3. Characterization of metal coated aperture probe at 780 nm of wavelength. (a) Incident angle θ_{inc} = 84 degrees, and the incident polarization (2θ) is controlled by rotating a λ/2 plate (θ). The transmitted light through the aperture is analyzed by rotating a linear polarizer at the end of probe fiber. (b) Incident polarization dependent transmission polarization. Projected incident electric (black line) and magnetic (red line) field polarizations on the flat-bottom plane of the probe are plotted together with the measured transmission polarization (circle). SEM image of the probe with flat-bottom apex (inset).

With the optically characterized metal coated probe which picks up the magnetic polarization component of light, the cross-section profile of the radially polarized beam is measured. Unlike the subwavelength aperture in a metal film, the aperture in the apex of the probe enables the various collection geometries which can easily exchange tangential and normal components of fields with respect to the aperture plane. Figure 4(a) describes experimental schematics where two different collection geometries, the front collection and the side collection, are used to test all the possible coupling schemes of the aperture probe with respect to the polarization direction of light.

From each collection geometry, coupled light into the aperture of the probe is guided through an optical fiber to be detected by a single photon counting module (SPCM-AQR-14, Perkin-Elmers) positioned at the end of the fiber. Section A-A' represents the polarizations of the electric (red arrow) and magnetic (blue arrow) fields at the focal spot. We now define the electric and magnetic tangential field components parallel to the aperture plane as E_{tan} and H_{tan} and the components normal to the aperture plane as E_{norm} and H_{norm}, respectively. In the front collection mode (Fig. 4(b)), the image shows a clear donut shape with dark center even though the z-polarized electric field E_{norm} is very strong at the center as seen by the polarization analyzed scattering experiments (Fig. 4(c)) which can detect local electric field of light [13]. The field strength of E_{norm} at the center is expected to be as large as about 60% of total electric field strength at the radial part of donut, according to the field profile calculation of radially polarized beam. This indicates that our aperture probe in the collection mode indeed does not detect the normal electric field E_{norm}, most likely because the dipole radiation is forbidden towards its own axis.

#181418 - $15.00 USD Received 10 Dec 2012; revised 16 Jan 2013; accepted 23 Jan 2013; published 28 Feb 2013

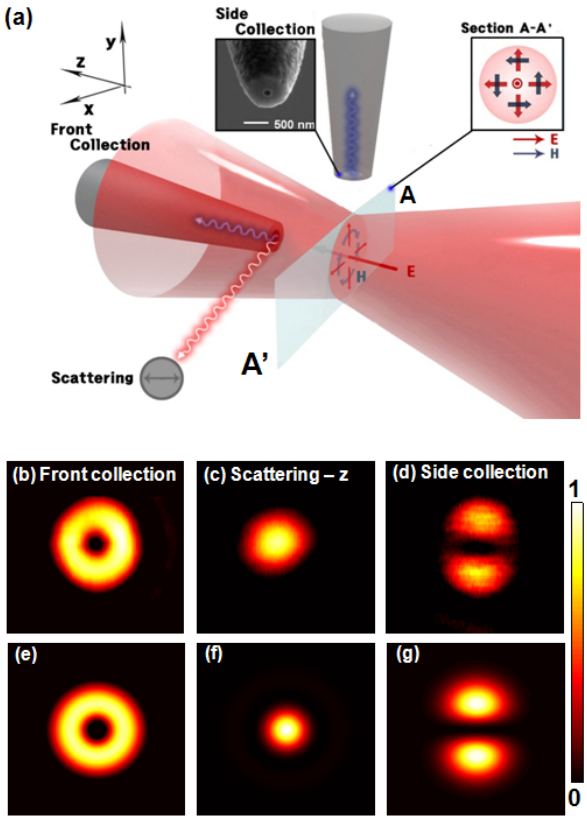

Fig. 4. (a) Experimental setup for characterization of a metal coated probe aperture. Radially polarized light with wavelength of 780 nm is focused using an x60 objective lens with the incident beam waist of 1.2 mm. The electric field (red arrows) and the magnetic field (blue arrows) distributions of the radially polarized light at the focal spot are also shown (section A-A'). Images of the radially polarized light scanned in a 5 μm x 5 μm area around focus region (b) in the front collection, (c) in the scattering and (d) in the side collection mode. The calculated field intensity distributions of (e) the tangential magnetic field and (f) the normal electric field, both for the front collection geometry, and (g) the tangential magnetic field for the side collection geometry.

The scanning image in the side collection mode (Fig. 4(d)) shows two lobes at upper and lower sides. Comparing this image to the polarization map shown in section A-A' of Fig. 4(a), the bright regions correspond to the strong H_{tan} and E_{norm}, whereas the dark regions correspond to E_{tan} and H_{norm}. Combining this result with the earlier discussion on Fig. 4(b) (E_{norm} is not coupled to the tip), we can unambiguously show that our tip is most strongly coupled to H_{tan} in the far-field regime. We estimate the contamination coupling of at most 25% from all the other components except H_{tan}, for example H_{norm}, E_{tan} and E_{norm}, based on the background analysis of side collected radially polarized beam (Fig. 4(d)). Our results are in good agreements with calculated field distributions [29] in Figs. 4(e), 4(f), and 4(g).

Now we proceed to measure the magnetic and electric fields of surface bounded SPP standing wave. Since SPP plays a crucial role in optical phenomena in metallic nano-structure, local measurement of SPP magnetic field is of particular interest in fabricating metamaterial which can be selectively designed to have dark or bright resonance mode [30–33]. SPP standing wave on a flat metal surface is generated by a 300 nm wide double slits with a 50 μm separation between them, which are punctured in a 150 nm thick gold film. Phase difference between electric and magnetic field polarizations of sinusoidal SPP standing wave can be used

#181418 - $15.00 USD Received 10 Dec 2012; revised 16 Jan 2013; accepted 23 Jan 2013; published 28 Feb 2013

to check the field components collected through the probe [34]. The slits are illuminated from the bottom by a 770 nm wavelength Ti:sapphire laser polarized along the x-axis. A metal coated aperture probe in dual mode NSOM [35] collects the magnetic field intensity, while the electric field intensity scattered by the apex of the same probe is measured in the far-field [13] (Fig. 5(a)). The scattering mode measurement is polarization resolved by placing a linear polarizer in front of the detector. SPP possesses three mutually orthogonal, spatially and temporally sinusoidal field components: transverse magnetic H_y, transverse electric E_z, and finally the longitudinal electric field E_x which makes SPP waves non-transverse. Symmetries in the sample geometry and the excitation dictate that the magnetic field of SPP standing wave is along tangential y-axis only. Consider H_y of the excited SPP standing wave in air,

$$H_y = H_0 \exp(ik_{spp}x - \kappa z) + H_0 \exp(-ik_{spp}x - \kappa z) = 2H_0 \cos(k_{spp}x)e^{-\kappa z} \qquad (1)$$

where k_{spp} is the wave vector along the x-direction, κ the spatial decay coefficient of SPP in the normal direction, and H_0 the magnetic field amplitude of SPP. The relation between k_{spp} and κ is determined by Helmholtz equation $(\omega_0/c)^2 = k_0^2 = k_{spp}^2 - \kappa^2$, where c is the speed of light. By Maxwell's equations, the normal electric field E_z is written:

$$E_z = -(2ik_{spp}H_0 / \omega\varepsilon_0)\sin(k_{spp}x)e^{-\kappa z} \qquad (2)$$

with permittivity of vacuum ε_0. The tangential magnetic field H_y (Eq. (1) and the normal electric field E_z (Eq. (2) are 90 degree out of phase and therefore completely out of phase in intensity. Figures 5(b), 5(c) and 5(d) show the intensity profile of SPP standing wave measured by collection, x-polarized scattering, and z-polarized scattering modes, respectively. Phase differences between SPP standing wave measured by collection and scattering modes are clearly revealed in the cross section profiles as shown in Figs. 5(e) and 5(f). Plot of analytic solution of SPP standing wave intensity (Eq. (1) and 2) is showing good consistency with the measurement (Fig. 5(g)). It should be noted that the field profile measured by the collection mode is shifted along the x-axis to calibrate the discrepancy in the positions of the scattering center and the aperture of the probe. This discrepancy can be attributed to the blunt probe apex with thick metal coating. For the calibration, the difference between the positions of the peak and dip of the intensity profile on the single slit opening are measured by collection and scattering modes, respectively. Since the electric and magnetic field parallel to the metal plane have maximum intensity at the center of the slit while the vertical electric field have the minimum intensity at the same position, we can experimentally determine the discrepancy in the positions of the scattering center and the aperture center of the probe. After the calibration, the standing wave pattern measured by collection mode is out of phase from the z-polarized scattering signal, consistent with the theoretical SPP standing wave analysis that predicts the normal electric field E_{norm} and the tangential magnetic fields H_{tan} are 90 degree out of phase [36] as shown in Eqs. (1) and (2).

#181418 - $15.00 USD Received 10 Dec 2012; revised 16 Jan 2013; accepted 23 Jan 2013; published 28 Feb 2013

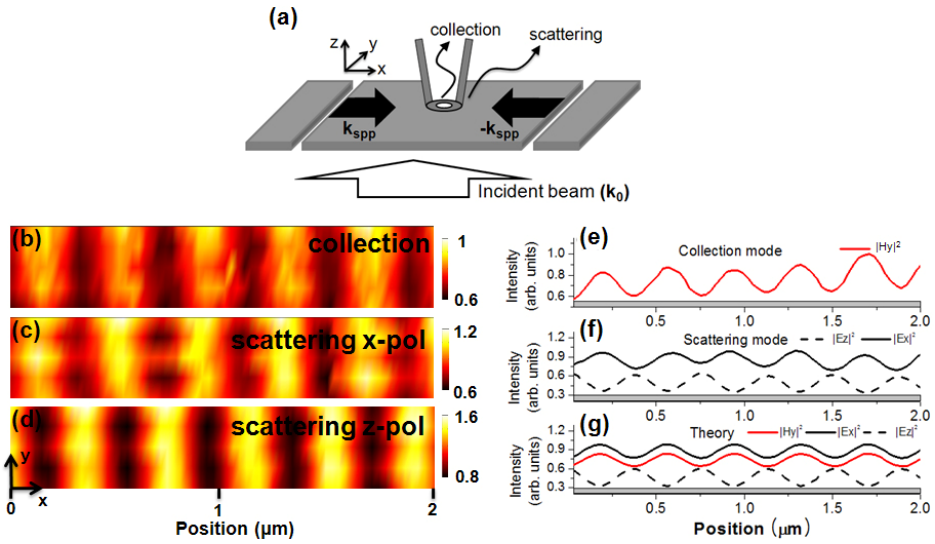

Fig. 5. (a) Schematic for SPP standing wave mapping on a gold film using a metal coated probe with a subwavelength aperture. 770 nm wavelength laser is illuminated from the back side of the sample with polarization orthogonal to the slit axis. Optical field intensity profile with periodicity of 381 nm measured by (b) collection mode, (c) scattering mode with the analyzing linear polarizer set along x-axis, and (d) z-axis. Cross section of intensity profile measured by (e) collection mode, (f) scattering mode with the analyzing linear polarizer set along z-axis (dashed) and x-axis (solid). (g) Electric and magnetic field intensity profiles derived from analytic solution of SPP standing wave.

3. Conclusions

In conclusion, we demonstrate the optical magnetic field visualization facilitated by a subwavelength aperture in a metal plane. The aperture punctured in a metal film or in the apex of a conical shaped probe is used to raster scan the cross-section of radially or azimuthally polarized beams to reveal the magnetic field intensity profiles. Furthermore, the aperture probe is used for local mapping of electric and magnetic fields of SPP in the near-field regime. We foresee a wide usage of subwavelength apertures for the full characterization of both electric and magnetic field components. Such technique will benefit the optical metamaterial development which requires engineering of local electric permittivity and magnetic permittivity on nanometer scales.

Acknowledgment

This work was supported by the National Research Foundation of Korea (NRF) grant funded by the Korean government (MEST) (SRC, No: 2008-0062255) (GRL, No: K20815000003) (Others, No: 2010-0029648, 2011-0019170, 2011-0020209), the Global Frontier R&D Program on Center for Multiscale Energy System (2012M3A6A7054864), and Hi Seoul Science / Humanities Fellowship from Seoul Scholarship Foundation.

#181418 - $15.00 USD Received 10 Dec 2012; revised 16 Jan 2013; accepted 23 Jan 2013; published 28 Feb 2013